Final Draft
of the original manuscript:

Mosler, J.; Cirak, F.:

A variational formulation for finite deformation wrinkling analysis of inelastic membranes

A variational formulation for finite deformation wrinkling analysis of inelastic membranes

Jörn Mosler [a],* and Fehmi Cirak [b]

[a]*GKSS Research Centre, Institute for Materials Research, Materials Mechanics, D-21502 Geesthacht, Germany*

[b]*Department of Engineering, University of Cambridge, Trumpington Street, Cambridge, CB2 1PZ, United Kingdom*

Abstract

This paper is concerned with a novel, fully variational formulation for finite deformation analysis of inelastic membranes with wrinkling. In contrast to conventional approaches, every aspect of the physical problem derives from minimization of suitable energy functionals. A variational formulation of finite strain plasticity theory, which leads to a minimization problem for the constitutive updates, serves as the starting point for the derivations. In order to take into account the kinematics induced by wrinkles and slacks, a relaxed version of the finite strain functional is postulated. In effect, the local incremental stress-strain relations are established via differentiation of the relaxed energy functional with respect to the strains. Hence, the presented formulation is fully analogous to that of hyperelasticity with the sole exception that the aforementioned functional depends on history variables and, accordingly, it is path dependent. The advantages associated with the developed variational method are manifold. From a practical point of view, the possibility of applying standard optimization algorithms to solve the minimization problem describing inelastic membranes is remunerative. From a mathematical point of view, on the other hand, the energy of the system induces some sort of natural metric representing an essential requirement for error estimation and thus, for adaptive finite element methods. The presented derivation of the model allows to consider possible material symmetries in the elastic as well as plastic response of the material. As a prototype, a von Mises-type model is implemented. The efficiency and performance of the resulting algorithm are demonstrated by means of numerical examples.

Key words: Finite strain plasticity, Wrinkling, Membranes, Finite element method, Variational principles, Energy relaxation, Variational constitutive updates
PACS:

* Tel.: +49-4152-87-2679; Fax.: +49-4152-87-2595
  Email address: `Joern.Mosler@gkss.de` (Jörn Mosler).

1 Introduction

Membranes are ubiquitous structural members in a number of engineering applications ranging from light-weight roofs in civil engineering, airbags in automobiles, solar sails and sunshields in aerospace engineering to stents in bio-engineering. Although the listed applications are relatively new, mechanical models for membranes go at least back to the works of Wagner [1] and Reissner [2] in the 30s. In [1,2] it is assumed that the membrane has no bending stiffness and, hence, cannot carry compressive stresses. This assumption leads directly to the celebrated *tension field theory* by Wagner, which has been elaborated upon by a number of researchers, cf., e.g. [3–9]. A comprehensive overview of the work carried out on tension field theory prior to 1990 can be found in [10] and references cited therein.

Despite the considerable success of the classical *tension field theory* in analytical case-by-case investigation and computational analysis of membranes structures, its numerical implementation is not straightforward. In particular for finite deformations, it leads to ambiguities with respect to the loading and unloading conditions, or in other terms, the wrinkling criteria. More precisely, once wrinkling occurs, the resulting stress field can indeed be computed by applying tension field theory, however, the theory does not provide any information if such a wrinkle forms. Hence, an additional criterion is needed, which is usually based on principal strains, principal stresses or a combination of both, cf. [7,8]. Clearly, since these loading conditions are often introduced in ad-hoc manner, there is no guarantee that they comply well with the tension field theory. As a consequence, the resulting boundary value problem is not continuous in general. Evidently, this is not physical and gives rise to numerical problems as well.

Alternatively, a fully variational strategy suitable for the analysis of wrinkles and slacks in membranes was proposed in a series of papers by Pipkin, cf. [11–13], see also [14]. Pipkin analyzed the energy of a membrane under certain assumptions and proved that the quasi-convexification of the Helmholtz energy defines a relaxed energy functional whose derivatives yield the membrane stresses, i.e., the stresses predicted by this relaxed potential fulfill the restrictions imposed by tension field theory. Interestingly, and in contrast to classical tension field theory, Pipkin's method inherently includes physically sound loading and unloading conditions; additional ad-hoc assumptions are not necessary. As a consequence, the resulting boundary value is continuous (more precisely, sufficiently smooth), which makes it physically and mathematically sound and convenient for numerical implementations.

Pipkin's ideas were further elaborated on by Mosler [15] in which a novel variational algorithmic formulation for wrinkling at finite strains was proposed. In line with Pipkin's original work [11–13], the unknown wrinkle distribution is computed by minimizing the Helmholtz energy of the membrane with respect to the wrinkling

parameters. The finite element model [15] allows to employ arbitrary, fully three-dimensional hyperelastic constitutive models directly. Furthermore, the plane stress conditions characterizing a membrane stress state are naturally included within the variational formulation.

In the present paper, the method advocated by Mosler [15] is extended to inelastic membranes. Although the ability to predict the deformations and ultimate load capacity of plastically deforming membranes is important, for example, for inflatable ETFE (Ethylene Tetra Fluoro Ethylene) cushions used in architecture [16] or sheet metal forming [17,18], only few numerical methods have been proposed yet, cf. [19,20]. In contrast to the cited references, the approach developed in this paper is fully variational, i.e., the wrinkling parameters, together with the plasticity related variables, follow from relaxing an incrementally defined potential and the stresses are computed simply by differentiating this functional. Thus, the relaxed potential is formally identical to that of standard hyperelasticity. Clearly, such a variational method shows several advantages compared to conventional strategies. For instance, it opens up the possibility of applying standard optimization algorithms to the numerical implementation, see [15]. This is especially important for highly non-linear or singular problems such as wrinkling. On the other hand, minimization principles provide a suitable basis for a posteriori error estimation and thus, for adaptive finite element formulations, cf. [21–23].

The paper is organized as follows: In Section 2, the fully variational wrinkling model proposed in [15] is briefly summarized. For the sake of simplicity, focus is on hyperelastic materials. Subsequently, a variational framework for finite strain plasticity theory is discussed in Section 3. In line with the wrinkling model, it allows to reformulate the elastoplastic constitutive update as a minimization problem. The key contribution of the present paper is elaborated in Section 4. More precisely, the minimization principles for wrinkling in elastic membranes and for plasticity in inelastic solids are combined to a novel variational approach for inelastic membranes. The performance of the resulting algorithmic formulation is demonstrated in Section 5.

2 Wrinkling in (hyper)elastic membranes

In this section, a summary of the variational formulation for wrinkling at finite strains based on energy minimization is presented. While Subsection 2.1 is concerned with the kinematics induced by slacks and wrinkles, details on the resulting variational strategy are given in Subsection 2.2. Further details may be found in the reference [15].

3

2.1 Kinematics

In the following, a membrane in its reference undeformed configuration is considered. Since a membrane represents a two-dimensional submanifold in the three-dimensional space, it can be conveniently characterized by an atlas. Hence, the reference configuration $\Omega \subset \mathbb{R}^3$ is (locally) defined by a chart $\tilde{\boldsymbol{X}} : \mathbb{R}^2 \supset \mathcal{U} \to \subset \mathcal{M} \subset \mathbb{R}^3$, $\theta_\alpha \mapsto \boldsymbol{X}$. The same concept can be applied to the description of the deformed configuration $\varphi(\Omega)$, i.e., $\tilde{\boldsymbol{x}} : \mathbb{R}^2 \supset \mathcal{U} \to \subset \mathcal{K} \subset \mathbb{R}^3$, $\theta_\alpha \mapsto \boldsymbol{x}$ with $\boldsymbol{X}$ and $\boldsymbol{x}$ being the position vectors of a point within the undeformed and the deformed configuration, respectively. Assuming that the charts are sufficiently smooth diffeomorphisms, the deformation mapping φ connecting $\boldsymbol{X}$ and $\boldsymbol{x}$ is well defined, i.e., $\varphi = \tilde{\boldsymbol{x}} \circ \tilde{\boldsymbol{X}}^{-1}$ and the deformation gradient yields $\boldsymbol{F} := \partial \tilde{\boldsymbol{x}} / \partial \theta_\alpha \otimes \partial \theta_\alpha / \theta \tilde{\boldsymbol{X}}$. Based on $\boldsymbol{F}$ the right Cauchy-Green strain tensor $\boldsymbol{C} = \boldsymbol{F}^T \cdot \boldsymbol{F}$ can be computed. $\boldsymbol{C}$ is a symmetric ($\boldsymbol{C} = \boldsymbol{C}^T$) and positive definite ($\boldsymbol{C} > 0$) second-order tensor. It is noteworthy that for membranes, the deformation gradient $\boldsymbol{F}$ as well as the strain tensor $\boldsymbol{C}$ can be represented by 2×2 tensors without loss of generality, despite $\mathcal{M} \subset \mathbb{R}^3$ and $\mathcal{K} \subset \mathbb{R}^3$, cf. [12,6]. However, since in this paper fully three-dimensional constitutive models will be considered, a three-dimensional strain state is required. Using the spectral decomposition theorem, $\boldsymbol{C}$ can be written in the following form:

$$\boldsymbol{C} = (\lambda_1^C)^2 \, \boldsymbol{N}_1 \otimes \boldsymbol{N}_1 + (\lambda_1^C)^2 \, \boldsymbol{N}_2 \otimes \boldsymbol{N}_2 + (\lambda_3^C)^2 \, \boldsymbol{N}_3 \otimes \boldsymbol{N}_3, \tag{1}$$

where the orthogonal unit eigenvectors $\boldsymbol{N}_1$ and $\boldsymbol{N}_2$ are in the tangent space of the undeformed membrane surface while the unit vector $\boldsymbol{N}_3$ is normal $\boldsymbol{N}_1$ and $\boldsymbol{N}_2$. Thereby, it is assumed that the out-of-plane shear strains of the membrane are zero.

So far, the kinematics induced by wrinkles have not been taken into account. In general, wrinkling can either be modeled explicitly using thin shell models [24], or in a smeared fashion [15]. Here, the focus is on the latter approach which is particularly useful in presence of fine wrinkling. More precisely, the additional out-of-plane component of the deformation mapping due to wrinkles is captured by a right Cauchy-Green tensor $\boldsymbol{C}_\mathrm{w}$. Consequently, the effective or relaxed strain tensor $\boldsymbol{C}_\mathrm{r}$ reads

$$\boldsymbol{C}_\mathrm{r} = \boldsymbol{C} + \boldsymbol{C}_\mathrm{w}. \tag{2}$$

As shown in [13,20,15], the wrinkling-related part $\boldsymbol{C}_\mathrm{w}$ can be decomposed according to

$$\boldsymbol{C}_\mathrm{w} = a^2 \, \boldsymbol{N} \otimes \boldsymbol{N} \tag{3}$$

with $\boldsymbol{N}$ being the wrinkling direction and the scalar a depends on the frequency and amplitudes of the wrinkles. According to Eq. (3), $\boldsymbol{C}_\mathrm{w}$ is semi-positive definite

$(\boldsymbol{C}_{\mathrm{w}} \geq 0)$ and hence, $\boldsymbol{C}_{\mathrm{r}} > 0$.

If wrinkles and slacks are to be modeled, a slight modification of the kinematics is necessary. Conceptionally, slacks can be understood as two orthogonal wrinkles which lead to

$$\boldsymbol{C}_{\mathrm{w}} = a^2 \, \boldsymbol{N} \otimes \boldsymbol{N} + b^2 \, \boldsymbol{M} \otimes \boldsymbol{M}, \tag{4}$$

cf. [15]. Here, the orthogonal vectors $\boldsymbol{N}$ and $\boldsymbol{M}$ span the tangent space of the undeformed membrane. Obviously, $\boldsymbol{C}_{\mathrm{w}}$ is identical to Eq. (3), if b equals zero. Otherwise, $\boldsymbol{C}_{\mathrm{w}}$ corresponds to a slack. Interestingly, if $\boldsymbol{C}_{\mathrm{w}}$ is interpreted as a 2×2 tensor (within the tangent space of Ω), any symmetric semi-positive definite tensor can be generated by varying a, b and $\boldsymbol{N}$. As a result, the relaxed strain tensor can be re-written as

$$\boldsymbol{C}_{\mathrm{r}} = \boldsymbol{C} + \boldsymbol{C}_{\mathrm{w}}, \qquad \boldsymbol{C}_{\mathrm{w}} \geq 0, \tag{5}$$

cf. [13]. Again, $\boldsymbol{C}_{\mathrm{w}} \geq 0$ denotes that $\boldsymbol{C}_{\mathrm{w}}$ is semi-positive definite.

2.2 A variational formulation for wrinkling at finite strains based on energy minimization

For the sake of clarity, attention is focused on wrinkling in (hyper)elastic materials first. In this case, a strain energy functional $\Psi = \Psi(\boldsymbol{C})$ exists and the first Piola-Kirchhoff stress tensor $\boldsymbol{P}$ and the second Piola-Kirchhoff stresses $\boldsymbol{S}$ are computed as

$$\boldsymbol{P} = 2 \, \boldsymbol{F} \cdot \frac{\partial \Psi}{\partial \boldsymbol{C}} \qquad \boldsymbol{S} = 2 \, \frac{\partial \Psi}{\partial \boldsymbol{C}}. \tag{6}$$

Furthermore, it is assumed that the reference configuration is stress free (locally), i.e.,

$$\Psi(\boldsymbol{C} = \boldsymbol{1}) = 0, \qquad \boldsymbol{P}(\boldsymbol{C} = \boldsymbol{1}) = \boldsymbol{0}. \tag{7}$$

It is well known that for such material models the deformation mapping $\boldsymbol{\varphi}$ can be computed by applying the principle of minimum potential energy, i.e.,

$$\boldsymbol{\varphi} = \arg \inf_{\boldsymbol{\varphi}} I(\boldsymbol{\varphi}), \tag{8}$$

5

with

$$I(\boldsymbol{\varphi}) := \int_\Omega \Psi(\boldsymbol{C}) \, \mathrm{d}V - \int_\Omega \boldsymbol{B} \cdot \boldsymbol{\varphi} \, \mathrm{d}V - \int_{\partial\Omega_2} \bar{\boldsymbol{T}} \cdot \boldsymbol{\varphi} \, \mathrm{d}A. \tag{9}$$

Here, $\boldsymbol{B}$ and $\bar{\boldsymbol{T}}$ represent prescribed body forces and tractions acting on $\partial\Omega_2$. Obviously, $\boldsymbol{\varphi}$ has to comply with the essential boundary conditions imposing additional restrictions in the resulting minimization problem. Clearly, if principle (8) is directly employed, physically inadmissible compressive membrane stresses may occur.

According to the previous subsection, wrinkles or slacks can be taken into account by modifying the right Cauchy-Green tensor. Thus, the potential energy of a membrane is given simply by replacing the standard strain tensor $\boldsymbol{C}$ in Eq. (9) by its relaxed counterpart, cf. Eq. (2). Denoting now the deformation of the middle plane of the membrane as $\boldsymbol{\varphi}$, the energy of a hyperelastic membrane reads

$$I(\boldsymbol{\varphi}, \lambda_3^{\boldsymbol{C}}, a, b, \alpha) := \int_\Omega \Psi(\boldsymbol{C}_{\mathrm{r}}(\boldsymbol{\varphi}, \lambda_3^{\boldsymbol{C}}, a, b, \alpha)) \, \mathrm{d}V - \int_\Omega \boldsymbol{B} \cdot \boldsymbol{\varphi} \, \mathrm{d}V - \int_{\partial\Omega_2} \bar{\boldsymbol{T}} \cdot \boldsymbol{\varphi} \, \mathrm{d}A. \tag{10}$$

In Eq. (10), α represents an angle which defines the vectors $\boldsymbol{N} = [\cos\alpha; \ \sin\alpha]^T$ and $\boldsymbol{M} = [-\sin\alpha; \ \cos\alpha]^T$ (the normal vector $\boldsymbol{N}_3$ is known in advance). Since energy minimization is the overriding principle governing every aspect of the mechanical problem under investigation, it is natural to postulate that wrinkles and slacks form such that they lead to the energetically most favorable state:

$$(\boldsymbol{\varphi}, \lambda_3^{\boldsymbol{C}}, a, b, \alpha) = \arg \inf_{\boldsymbol{\varphi}, \lambda_3^{\boldsymbol{C}}, a, b, \alpha} I(\boldsymbol{\varphi}, \lambda_3^{\boldsymbol{C}}, a, b, \alpha). \tag{11}$$

Since the variables a, b, α and $\lambda_3^{\boldsymbol{C}}$ are locally defined, the minimization problem (11) can be decomposed into two consecutive optimization problems. First, for a given deformation mapping, the parameters a, b, α and $\lambda_3^{\boldsymbol{C}}$ are computed from the local minimization problem

$$(\lambda_3^{\boldsymbol{C}}, a, b, \alpha) := \arg \inf_{\lambda_3^{\boldsymbol{C}}, a, b, \alpha} \Psi(\boldsymbol{\varphi}, \lambda_3^{\boldsymbol{C}}, a, b, \alpha) \tag{12}$$

which defines a relaxed energy functional

$$\Psi_{\mathrm{r}}(\boldsymbol{C}(\boldsymbol{\varphi})) = \inf_{\lambda_3^{\boldsymbol{C}}, a, b, \alpha} \Psi(\boldsymbol{\varphi}, \lambda_3^{\boldsymbol{C}}, a, b, \alpha) \tag{13}$$

6

depending only on the deformation mapping. It can be shown that the stationarity conditions associated with the minimization problem (12) are given by

$$
\begin{aligned}
\frac{\partial \Psi}{\partial \lambda_3^C} &= 0 \iff \lambda_3^C \, S_{33} = 0 && \iff \sigma_{33} = 0 \\
\frac{\partial \Psi}{\partial a} &= 0 \iff a \, S_{NN} = 0 && \iff S_{NN} = 0 \ \ (\text{if } a \neq 0) \\
\frac{\partial \Psi}{\partial b} &= 0 \iff b \, S_{MM} = 0 && \iff S_{MM} = 0 \ (\text{if } b \neq 0) \\
\frac{\partial \Psi}{\partial \alpha} &= 0 \iff (a^2 - b^2) \, S_{NM} = 0 \iff S_{NM} = 0 \ (\text{if } a \neq 0 \text{ or } b \neq 0),
\end{aligned} \tag{14}
$$

cf. [15]. Here, $\boldsymbol{\sigma}$ are the Cauchy stresses and $S_{NN} := \boldsymbol{S} : (\boldsymbol{N} \otimes \boldsymbol{N})$, $S_{NM} := \boldsymbol{S} : (\boldsymbol{N} \otimes \boldsymbol{M})$ and $S_{MM} := \boldsymbol{S} : (\boldsymbol{M} \otimes \boldsymbol{M})$ with the second Piola-Kirchhoff stresses $\boldsymbol{S} = 2 \, \partial_{\boldsymbol{C}_{\mathrm{r}}} \Psi$. Accordingly, plane stress conditions are naturally included within the variational formulation (note that the out-of-plane shear strains vanish). Furthermore, in case of wrinkling ($a \neq 0$, $b = 0$), the resulting stress state is one-dimensional, i.e., $S_{NN} = 0$, $S_{NM} = 0$, while the stresses vanish completely, if a slack forms. Further details of the stationary conditions (14) the can be found in [15].

Once the local problem (13) has been solved, the deformation mapping follows from the following minimization problem on the structure level:

$$
\boldsymbol{\varphi} = \arg \inf_{\boldsymbol{\varphi}} \left[\int_{\Omega} \Psi_{\mathrm{r}}(\boldsymbol{C}) \, \mathrm{d}V - \int_{\Omega} \boldsymbol{B} \cdot \boldsymbol{\varphi} \, \mathrm{d}V - \int_{\partial \Omega_2} \bar{\boldsymbol{T}} \cdot \boldsymbol{\varphi} \, \mathrm{d}A \right]. \tag{15}
$$

It bears emphasis that both problems (12) and (15) can be computed by using standard optimization algorithms. For the spatial discretization of Eq. (15) the finite element method is used.

Remark 1 *If Ψ is an isotropic tensor function, the minimization problem (12) can be solved semi-analytically. More precisely, a variation with respect to the wrinkling parameters a and b yields $\boldsymbol{M} = \boldsymbol{N}_1$ and $\boldsymbol{N} = \boldsymbol{N}_2$ with $\lambda_1^C > \lambda_2^C$. Hence, $\boldsymbol{C}$ and $\boldsymbol{C}_{\mathrm{w}}$ are coaxial and the wrinkling directions are known in advance. Furthermore, in case of wrinkling (no slacks), the resulting stress state is one-dimensional and hence, two of the eigenvalues of $\boldsymbol{C}_{\mathrm{r}}$ are identical ($\lambda_2^C = \lambda_3^C$). Consequently, the minimization problem (12) depends only on a, i.e., it is scalar-valued.*

3 Variational constitutive updates

This section is concerned with the so-called *variational constitutive updates*. Those updates allow to formulate a broad range of different plasticity or damage models as optimization problems similar to that of wrinkling (compare to Eq. (11)). As a prototype and for the sake of concreteness, attention is restricted to finite strain plasticity theory based on a multiplicative decomposition of the deformation gradient into elastic $\boldsymbol{F}^{\mathrm{e}}$ and plastic $\boldsymbol{F}^{\mathrm{p}}$ parts ($\boldsymbol{F} = \boldsymbol{F}^{\mathrm{e}} \cdot \boldsymbol{F}^{\mathrm{p}}$). Evidently, for path-dependent problems such as plasticity theory, the optimization problem is defined pointwise (with respect to the (pseudo) time). Throughout this section, the kinematics induced by wrinkles or slacks are not taken into account. The coupling of variational constitutive updates and the variational wrinkling algorithm in Section 2 will be discussed in Section 4. This section follows to a large extend the previous works [25–27]. An overview on the slightly different variational constitutive updates which can be found in the literature is given in [23].

3.1 Fundamentals

Focusing on plasticity models, the Helmholtz energy reads

$$\Psi(\boldsymbol{F}, \boldsymbol{F}^{\mathrm{p}}, \boldsymbol{\kappa}) = \Psi^{\mathrm{e}}(\boldsymbol{F}^{\mathrm{e}}) + \Psi^{\mathrm{p}}(\boldsymbol{\kappa}) \tag{16}$$

with $\boldsymbol{\kappa}$ being internal strain-like variables. While Ψ^{e} represents the elastic stored energy, the second term in Eq. (16) denotes the stored energy due to plastic work. It is associated with isotropic/kinematic hardening/softening. In case of so-called *standard dissipative solids* in the sense of Halphen & Nguyen [28], which are the cornerstone of variational constitutive updates, the material model is completely defined by means of only two scalar-valued functions. One of those is the Helmholtz energy, while the other, namely the yield function ϕ, spans the admissible stress space $\mathbb{E}_\sigma$, i.e.,

$$\mathbb{E}_\sigma := \{(\boldsymbol{\Sigma}, \boldsymbol{Q}) \in \mathbb{R}^{9 \times n} \mid \phi = \phi(\boldsymbol{\Sigma}, \boldsymbol{Q}) \leq 0\}, \qquad \boldsymbol{Q} := -\partial_{\boldsymbol{\kappa}} \Psi. \tag{17}$$

Here, $\boldsymbol{\Sigma}$ are the Mandel stresses and $\boldsymbol{Q}$ is a set of n internal stress-like variables conjugate to $\boldsymbol{\kappa}$. Assuming associativity, the flow rules and the evolution equations are obtained as

$$\boldsymbol{L}^{\mathrm{p}} := \dot{\boldsymbol{F}}^{\mathrm{p}} \cdot \boldsymbol{F}^{\mathrm{p}-1} = \lambda \underbrace{\partial_{\boldsymbol{\Sigma}} \phi}_{=: \boldsymbol{K}}, \qquad \dot{\boldsymbol{\kappa}} = \lambda \, \partial_{\boldsymbol{Q}} \phi. \tag{18}$$

The plastic multiplier λ in Eq. (18) has to fulfill the Karush-Kuhn-Tucker conditions

$$\lambda \geq 0, \quad \phi \leq 0, \quad \lambda\, \phi = 0. \tag{19}$$

For the derivation of variational constitutive updates, the potential

$$\tilde{\mathcal{E}}(\dot{\boldsymbol{\varphi}}, \dot{\boldsymbol{F}}^{\mathrm{p}}, \dot{\boldsymbol{\kappa}}, \boldsymbol{\Sigma}, \boldsymbol{Q}) = \dot{\Psi}(\dot{\boldsymbol{\varphi}}, \dot{\boldsymbol{F}}^{\mathrm{p}}, \dot{\boldsymbol{\kappa}}) + \mathcal{D}(\dot{\boldsymbol{F}}^{\mathrm{p}}, \dot{\boldsymbol{\kappa}}, \boldsymbol{\Sigma}, \boldsymbol{Q}) + J(\boldsymbol{\Sigma}, \boldsymbol{Q}) \tag{20}$$

is introduced with

$$\mathcal{D} = \boldsymbol{\Sigma} : \boldsymbol{L}^{\mathrm{p}} + \boldsymbol{Q} \cdot \dot{\boldsymbol{\kappa}} \geq 0 \tag{21}$$

being the (reduced) dissipation and $J(\boldsymbol{\Sigma}, \boldsymbol{Q})$ denotes the characteristic function of $\mathbb{E}_\sigma$, i.e.,

$$J(\boldsymbol{\Sigma}, \boldsymbol{Q}) := \begin{cases} 0 & \forall (\boldsymbol{\Sigma}, \boldsymbol{Q}) \in \mathbb{E}_{\boldsymbol{\sigma}} \\ \infty & \text{otherwise.} \end{cases} \tag{22}$$

According to Eq. (20), for admissible stress states, i. e., $(\boldsymbol{\Sigma}, \boldsymbol{Q}) \in \mathbb{E}_{\boldsymbol{\sigma}}$, $\tilde{\mathcal{E}}$ represents the sum of the rate of the stored energy and the dissipation, i.e., the stress power. Without going too much into detail, it can be shown that the stationarity conditions associated with Eq. (20) define the constitutive model completely, cf. [25–27]. For instance, a variation of Eq. (20) with respect to $\boldsymbol{\Sigma}$ yields the flow rule (18)$_1$. Finally, applying a Legendre transformation of the type

$$J^*(\bar{\boldsymbol{L}}^{\mathrm{p}}, \dot{\boldsymbol{\kappa}}) = \sup_{\boldsymbol{\Sigma}, \boldsymbol{Q}} \left\{ \boldsymbol{\Sigma} : \bar{\boldsymbol{L}}^{\mathrm{p}} + \boldsymbol{Q} \cdot \dot{\boldsymbol{\kappa}} \;\middle|\; (\boldsymbol{\Sigma}, \boldsymbol{Q}) \in \mathbb{E}_{\boldsymbol{\sigma}} \right\} \tag{23}$$

results in the reduced potential

$$\mathcal{E}(\dot{\boldsymbol{\varphi}}, \dot{\boldsymbol{F}}^{\mathrm{p}}, \dot{\boldsymbol{\kappa}}) = \dot{\Psi}(\dot{\boldsymbol{\varphi}}, \dot{\boldsymbol{F}}^{\mathrm{p}}, \dot{\boldsymbol{\kappa}}) + J^*(\dot{\boldsymbol{L}}^{\mathrm{p}}, \dot{\boldsymbol{\kappa}}) \tag{24}$$

(note that J^* is positively homogeneous of degree one). Hence, the only remaining variables are $\dot{\boldsymbol{\varphi}}$, $\dot{\boldsymbol{F}}^{\mathrm{p}}$ and $\dot{\boldsymbol{\kappa}}$. Even more importantly, the strain-like internal variables $\boldsymbol{F}^{\mathrm{p}}$ and $\boldsymbol{\kappa}$ follow jointly from the minimization principle

$$\overset{\circ}{\Psi}_{\mathrm{red}}(\dot{\boldsymbol{\varphi}}) := \inf_{\dot{\boldsymbol{F}}^{\mathrm{p}}, \dot{\boldsymbol{\kappa}}} \mathcal{E}(\dot{\boldsymbol{\varphi}}, \dot{\boldsymbol{F}}^{\mathrm{p}}, \dot{\boldsymbol{\kappa}}) \tag{25}$$

which, itself, gives rise to the introduction of the reduced functional $\overset{\circ}{\Psi}_{\mathrm{red}}$ depending only on the deformation mapping.

9

An effective numerical implementation can be simply obtained by applying a time discretization to Eq. (24), i.e.,

$$(\boldsymbol{F}^{\mathrm{p}}_{n+1}, \boldsymbol{\kappa}_{n+1}) = \arg \inf_{\boldsymbol{F}^{\mathrm{p}}_{n+1}, \boldsymbol{\kappa}_{n+1}} \int_{t_n}^{t_{n+1}} \mathcal{E}(\boldsymbol{\varphi}_{n+1}, \boldsymbol{F}^{\mathrm{p}}_{n+1}, \boldsymbol{\kappa}_{n+1}) \, \mathrm{d}t. \tag{26}$$

For the sake of concreteness and simplicity, yield functions which are positively homogeneous of degree one will be considered throughout the remaining part of this paper. In this case, the dissipation reads

$$\mathcal{D} = \lambda \, \sigma_0 = J^* \geq 0 \tag{27}$$

with J^* being the Legendre transformation of J. Consequently, if the stress state is admissible, the time discretization of Eq. (24) yields

$$\int_{t_n}^{t_{n+1}} \mathcal{E}(\boldsymbol{\varphi}_{n+1}, \boldsymbol{F}^{\mathrm{p}}_{n+1}, \boldsymbol{\kappa}_{n+1}) \, \mathrm{d}t = \Psi|_{t_{n+1}} - \Psi|_{t_n} + \Delta\lambda \, \sigma_0, \tag{28}$$

with $\Delta\lambda = \int_{t_n}^{t_{n+1}} \lambda \, \mathrm{d}t$. For the numerical integration of the evolution equations and the flow rule implicit schemes are applied. More precisely, the approximations

$$\boldsymbol{F}^{\mathrm{p}}_{n+1} \approx \exp[\Delta\lambda \, \boldsymbol{K}_{n+1}] \cdot \boldsymbol{F}^{\mathrm{p}}_n, \qquad \boldsymbol{\kappa}_{n+1} \approx \boldsymbol{\kappa}_n - \Delta\lambda \, \partial_{\boldsymbol{Q}}\phi|_{n+1} \tag{29}$$

are adopted.

Based on the numerical integrations (29) the optimization problem (26) can be solved. It defines, in turn, the reduced potential

$$\Psi_{\mathrm{inc}}(\boldsymbol{\varphi}_{n+1}) = \inf_{\boldsymbol{F}^{\mathrm{p}}_{n+1}, \boldsymbol{\kappa}_{n+1}} \int_{t_n}^{t_{n+1}} \mathcal{E}(\dot{\boldsymbol{\varphi}}, \dot{\boldsymbol{F}}^{\mathrm{p}}, \dot{\boldsymbol{\kappa}}) \, \mathrm{d}t. \tag{30}$$

Interestingly, if this potential is used within the standard principle of potential energy (8) and (9), the deformation mapping follows from the optimization problem

$$\boldsymbol{\varphi} = \arg \inf_{\boldsymbol{\varphi}} \left[\int_{\Omega} \Psi_{\mathrm{inc}}(\boldsymbol{\varphi}) \, \mathrm{d}V - \int_{\Omega} \rho_0 \, \boldsymbol{B} \cdot \boldsymbol{\varphi} \, \mathrm{d}V - \int_{\partial_2\Omega} \bar{\boldsymbol{T}} \cdot \boldsymbol{\varphi} \, \mathrm{d}A \right]. \tag{31}$$

As a result, plasticity theory formulated within the framework of standard dissipative solids is formally identical to the wrinkling algorithm as presented in the previous section (compare Eq. (26) to Eq. (12) and Eq. (31) to Eq. (15)).

10

Remark 2 *Suppose Ψ^{e} as well as ϕ are isotropic tensor functions (then, the Mandel stresses are symmetric). In this case, the elastic right Cauchy-Green tensor is coaxial to its trial counterpart. More precisely,*

$$\boldsymbol{C}^{\mathrm{etr}} := \boldsymbol{F}_n^{\mathrm{p}-T} \cdot \boldsymbol{C}_{n+1} \cdot \boldsymbol{F}_n^{\mathrm{p}-1} = \sum_{i=1}^{3} \left(\lambda_i^{\boldsymbol{C}^{\mathrm{etr}}}\right)^2 \, \boldsymbol{N}_i \otimes \boldsymbol{N}_i, \tag{32}$$

$$\boldsymbol{C}^{\mathrm{e}}{}_{n+1} := \boldsymbol{F}^{\mathrm{e}T}_{n+1} \cdot \boldsymbol{F}^{\mathrm{e}}_{n+1} = \sum_{i=1}^{3} \left(\lambda_i^{\boldsymbol{C}^{\mathrm{etr}}}\right)^2 \, \exp[-2\Delta\lambda_i^{\mathrm{p}}] \, \boldsymbol{N}_i \otimes \boldsymbol{N}_i. \tag{33}$$

Here, $\Delta\lambda_i^{\mathrm{p}}$ are the eigenvalues of $\Delta\lambda \, \boldsymbol{K}$, i.e.,

$$\Delta\lambda \, \boldsymbol{K} = \sum_{i=1}^{3} \Delta\lambda_i^{\mathrm{p}} \, \boldsymbol{N}_i \otimes \boldsymbol{N}_i. \tag{34}$$

Further details on the implementation of fully isotropic plasticity models can be found in [29].

3.2 Example I: single slip system – Tresca's flow rule

In case of single-crystal plasticity (in the sense of Schmid's law), the yield function ϕ is given by

$$\phi(\boldsymbol{\Sigma}, \kappa) = |\boldsymbol{\Sigma} : (\bar{\boldsymbol{m}} \otimes \bar{\boldsymbol{n}})| - Q(\kappa) - \sigma_0 \tag{35}$$

where the slip plane is defined by its corresponding normal vector $\bar{\boldsymbol{n}}$ and the slip direction $\bar{\boldsymbol{m}}$. Evidently, the vectors $\bar{\boldsymbol{n}}$ and $\bar{\boldsymbol{m}}$ are objects that belong to the intermediate configuration (induced by the multiplicative split $\boldsymbol{F} = \boldsymbol{F}^{\mathrm{e}} \cdot \boldsymbol{F}^{\mathrm{p}}$). Furthermore, $\bar{\boldsymbol{n}}$ and $\bar{\boldsymbol{m}}$ are orthogonal to one another and time-independent. Isotropic hardening/softening is taken into account by the yield stress Q depending on the strain-like internal variable κ. Accordingly, the associative flow rule reads

$$\boldsymbol{L}^{\mathrm{p}} = \tilde{\lambda} \, (\bar{\boldsymbol{m}} \otimes \bar{\boldsymbol{n}}), \quad \text{with} \quad \tilde{\lambda} = \lambda \, \mathrm{sign}\left[\boldsymbol{\Sigma} : (\bar{\boldsymbol{m}} \otimes \bar{\boldsymbol{n}})\right], \quad \lambda \geq 0 \tag{36}$$

while the evolution of the internal variable κ reduces to

$$\dot{\kappa} = \lambda \geq 0. \tag{37}$$

It is noteworthy that the flow rule can be integrated analytically yielding

$$\boldsymbol{F}_{n+1}^{\mathrm{p}} = (\boldsymbol{1} + \Delta\tilde{\lambda} \, \bar{\boldsymbol{m}} \otimes \bar{\boldsymbol{n}}) \cdot \boldsymbol{F}_n^{\mathrm{p}}. \tag{38}$$

As a result, by inserting Eq. (36) – (38) into Eq. (28), the resulting variational constitutive update (26) simplifies significantly, i.e.,

$$\Delta\tilde{\lambda} = \arg\inf_{\Delta\tilde{\lambda}} \left\{ \Psi_{n+1}(\boldsymbol{F}^{\mathrm{p}}_{n+1}(\Delta\tilde{\lambda}), \kappa_{n+1}(\Delta\tilde{\lambda})) - \Psi_n + |\Delta\tilde{\lambda}|\, \sigma_0 \right\}. \tag{39}$$

This scalar-valued problem can be numerically solved by using standard optimization strategies.

3.3 Example II: von Mises Plasticity

For the numerical example given in Section 5, a finite strain von Mises plasticity model is adopted. It is based on a yield function of the type

$$\phi(\boldsymbol{\Sigma}, \kappa) = ||\mathrm{sym}[\mathrm{dev}[\boldsymbol{\Sigma}]]||_2 - Q(\varepsilon^{\mathrm{p}}) - \sigma_0 \tag{40}$$

with the deviator $\mathrm{dev}[\boldsymbol{\Sigma}] = \boldsymbol{\Sigma} - 1/3\,[\boldsymbol{\Sigma} : \mathbf{1}]\,\mathbf{1}$ and the equivalent plastic strain ε^{p}. It is noteworthy that analogous to the model in the previous subsection, this yield function is positively homogeneous of degree one. Hence, the dissipation is given by $\mathcal{D} = \dot{\varepsilon}^{\mathrm{p}}\, \sigma_0 \geq 0$, provided the evolution equations are admissible, i.e.,

$$\dot{\boldsymbol{F}}^{\mathrm{p}} \cdot \boldsymbol{F}^{\mathrm{p}^{-1}} = \dot{\varepsilon}^{\mathrm{p}}\, \boldsymbol{K}, \quad \text{with} \quad \mathrm{tr}\boldsymbol{K} = 0, \quad \boldsymbol{K} = \boldsymbol{K}^T, \quad \frac{2}{3}\,\boldsymbol{K} : \boldsymbol{K} = 1, \quad \dot{\varepsilon}^{\mathrm{p}} \geq 0. \tag{41}$$

Further details may be found in [25] and [30]. Clearly, the conditions (41) impose additional restrictions in the resulting variational constitutive update (26). However, if the elastic energy Ψ^{e} is isotropic (which is the case for the numerical example in Section 5), the constraints (41) can be enforced a priori. This is briefly explained in what follows.

According to Remark 2, if Ψ^{e} and ϕ are isotropic tensor functions, the elastic right Cauchy-Green tensor is given by Eq. (33). Thus, restriction $\mathrm{tr}\boldsymbol{K} = 0$ can be enforced by setting

$$\sum_{i=1}^{3} \Delta\lambda_i^{\mathrm{p}} = 0 \quad \Rightarrow \quad \Delta\lambda_3^{\mathrm{p}} = -(\Delta\lambda_1^{\mathrm{p}} + \Delta\lambda_2^{\mathrm{p}}) \tag{42}$$

($\Delta\lambda_i^{\mathrm{p}}$ are the eigenvalues of $\Delta\lambda\,\boldsymbol{K}$). Finally, combining Eq. (42) with the normalizing condition Eq. $(41)_4$ yields

$$\Delta\varepsilon^{\mathrm{p}} = \sqrt{1/3}\, \sqrt{[\Delta\lambda_1^{\mathrm{p}}]^2 + [\Delta\lambda_2^{\mathrm{p}}]^2 + \Delta\lambda_1^{\mathrm{p}}\, \Delta\lambda_2^{\mathrm{p}}} \tag{43}$$

and consequently, the discretized optimization problem (26) reduces to

$$(\Delta\lambda_1^{\mathrm{p}}, \Delta\lambda_2^{\mathrm{p}}) = \arg\inf_{\Delta\lambda_1^{\mathrm{p}} \geq 0, \Delta\lambda_2^{\mathrm{p}} \geq 0} \{\Psi_{n+1}(\Delta\lambda_1^{\mathrm{p}}, \Delta\lambda_2^{\mathrm{p}}) - \Psi_n + \sigma_0\,\Delta\varepsilon^{\mathrm{p}}(\Delta\lambda_1^{\mathrm{p}}, \Delta\lambda_2^{\mathrm{p}})\}\,.\tag{44}$$

This version of the von Mises plasticity model has been employed within the numerical example shown in Section 5. It bears emphasis that plane stress condition can be enforced by considering a right Cauchy-Green tensor of the type (1) and minimizing Eq. (44) with respect to $\Delta\lambda_1^{\mathrm{p}}$, $\Delta\lambda_2^{\mathrm{p}}$ and additionally with respect to λ_3^C.

4 Wrinkling in inelastic membranes

In this section, the coupling of the kinematics induced by wrinkles or slacks according to Section 2.1 and variational constitutive updates as presented in Section 3 is discussed. For demonstration purposes two illustrative examples are given. While Subsection 4.4.1 is concerned with the combination of single-slip plasticity and wrinkles, details on the coupling of von Mises plasticity and membranes are given in Subsection 4.4.2.

4.1 Fundamentals

Since energy minimization is the overriding principle governing the formation of wrinkles or slacks as well as plastic deformations, it is suggestive to postulate that this principle even holds in the fully coupled case. Thus, the ultimate goal of this section is the derivation of such a variationally consistent approach.

For the derivation of the coupled model, the kinematics have to be modified first. Unfortunately, this coupling seems not to be uniquely defined. More precisely, with the elastoplastic split $\boldsymbol{F} = \boldsymbol{F}^{\mathrm{e}} \cdot \boldsymbol{F}^{\mathrm{p}}$ resulting in $\boldsymbol{C}^{\mathrm{e}} = \boldsymbol{F}^{\mathrm{e}T} \cdot \boldsymbol{F}^{\mathrm{e}}$ and the wrinkling-related decomposition $\boldsymbol{C}_{\mathrm{r}} = \boldsymbol{C} + \boldsymbol{C}_{\mathrm{w}}$ the following physically sound, effective or relaxed elastic right Cauchy-Green strain tensors are admissible:

$$\boldsymbol{C}_{\mathrm{r}}^{\mathrm{e}} := \boldsymbol{C}^{\mathrm{e}} + \boldsymbol{C}_{\mathrm{w}}, \qquad \boldsymbol{C}^{\mathrm{e}} = \boldsymbol{F}^{\mathrm{e}T} \cdot \boldsymbol{F}^{\mathrm{e}}, \quad \boldsymbol{C}_{\mathrm{w}} = \boldsymbol{C}_{\mathrm{w}}^{T} \geq 0 \tag{45}$$

and

$$\boldsymbol{C}_{\mathrm{r}}^{\mathrm{e}} := \boldsymbol{F}^{\mathrm{p}-T} \cdot \left[\boldsymbol{C} + \tilde{\boldsymbol{C}}_{\mathrm{w}}\right] \cdot \boldsymbol{F}^{\mathrm{p}-1} = \boldsymbol{C}^{\mathrm{e}} + \boldsymbol{F}^{\mathrm{p}-T} \cdot \tilde{\boldsymbol{C}}_{\mathrm{w}} \cdot \boldsymbol{F}^{\mathrm{p}-1}, \quad \tilde{\boldsymbol{C}}_{\mathrm{w}} = \tilde{\boldsymbol{C}}_{\mathrm{w}}^{T} \geq 0.\tag{46}$$

However, since the plastic deformation gradient has only strictly positive eigenval-

ues, the equivalence

$$\tilde{C}_\text{w} = \tilde{C}_\text{w}^T \geq 0 \quad \Leftrightarrow \quad F^{\text{p}-T} \cdot \tilde{C}_\text{w} \cdot F^{\text{p}-1} =: C_\text{w} = C_\text{w}^T \geq 0 \tag{47}$$

holds. Consequently, both splits (45) and (46) are fully equivalent. Therefore and without loss of generality, the first decomposition is used in the following.

Replacing the standard elastic right Cauchy-Green strain tensor C^e by its relaxed counterpart C_r^e, the Helmholtz energy of an elastoplastic membrane is obtained as

$$\Psi = \Psi^\text{e}(C_\text{r}^\text{e}) + \Psi^\text{p}(\kappa). \tag{48}$$

As a consequence, the (relaxed) coupled minimization problem is now defined by

$$(F_{n+1}^\text{p}, \kappa_{n+1}, C_\text{w}) = \arg\inf_{F_{n+1}^\text{p}, \kappa_{n+1}, C_\text{w}} \int_{t_n}^{t_{n+1}} \mathcal{E}(\varphi_{n+1}, F_{n+1}^\text{p}, \kappa_{n+1}, C_\text{w}) \, \mathrm{d}t \tag{49}$$

compare to Eq. (26). Clearly, by setting $C_\text{w} = 0$ the standard elastoplastic case is recovered, while for $(F_{n+1}^\text{p}, \kappa_{n+1}) = 0$ the optimization problem reduces to the variational wrinkling model as presented in Section 2. The numerical implementation of the minimization problem (49) is elaborated in the next subsection.

4.2   Numerical implementation

For the numerical implementation, it is convenient to replace the optimization problem (49) by the equivalent problem

$$(F_{n+1}^\text{p}, \kappa_{n+1}, a, b, \alpha, \lambda_3^C) = \arg\inf_{F_{n+1}^\text{p}, \kappa_{n+1}, a, b, \alpha, \lambda_3^C} \int_{t_n}^{t_{n+1}} \mathcal{E} \, \mathrm{d}t \tag{50}$$

cf. Eq. (4). Here, it has been assumed that the considered constitutive model is fully three-dimensional and plane stress conditions are variationally enforced. If the model already fulfills plane stress conditions, the optimization problem (50) does not depend on the out-of-plane strain component λ_3^C. In what follows, attention is restricted to positively homogeneous yield functions of degree one. Hence, the dissipation reads $\mathcal{D} = \lambda \, \sigma_0 \geq 0$ (if the stresses and evolution equations are admissible) and thus

$$\int_{t_n}^{t_{n+1}} \mathcal{E} \, \mathrm{d}t = \Psi|_{t_{n+1}}(F_{n+1}^\text{p}, \kappa_{n+1}, a, b, \alpha, \lambda_3^C) - \Psi|_{t_n} + \Delta\lambda(F_{n+1}^\text{p}, \kappa_{n+1}) \, \sigma_0. \tag{51}$$

14

Clearly, a variation of $\int_{t_n}^{t_{n+1}} \mathcal{E} \, dt$ with respect to the wrinkling parameters (a, b, α) and λ_3^C yields the stationarity conditions (14) with the sole exception that the second Piola-Kirchhoff stresses $\boldsymbol{S} = 2 \, \partial_{\boldsymbol{C}_r} \Psi$ are replaced by their counterparts $\bar{\boldsymbol{S}} := 2 \, \partial_{\boldsymbol{C}_r^e} \Psi$. As a consequence, the variational problem (51) indeed enforces plane stress conditions and wrinkling is characterized by a one-dimensional stress state. In case of slacks, the stresses vanish completely. Furthermore, since

$$\frac{\partial \boldsymbol{C}_r^e}{\partial \boldsymbol{C}^e} = \mathbb{I}^{\mathrm{sym}} \tag{52}$$

the stationarity conditions corresponding to a variation of $\int_{t_n}^{t_{n+1}} \mathcal{E} \, dt$ with respect to the plastic variables $\boldsymbol{F}^p$ and $\boldsymbol{\kappa}$ have the same physical interpretations as those of the standard model (without wrinkles or slacks) as explained in Section 3. As a result, wrinkles and slacks in inelastic membranes (more precisely, in standard dissipative solids) are, as a matter of fact, governed by energy minimization, cf. Eq. (50).

In principle, minimization problem (50) could be solved by using standard optimization algorithms. However, that would be numerically relatively expensive. Furthermore, the problem is not $\mathcal{C}^1$-smooth with respect to the plastic variables. For that reason, a coupled predictor-corrector method is applied, cf. [31,29]. Denoting the trial state of $(\bullet)$ as $(\bullet)^{\mathrm{tr}}$, the elastic, relaxed trial strains are defined as

$$[\boldsymbol{C}_r^e]^{\mathrm{tr}} := \boldsymbol{F}_n^{p-T} \cdot \boldsymbol{C}_{n+1} \cdot \boldsymbol{F}_n^{p-1}. \tag{53}$$

Accordingly, the trial state is characterized by a purely elastic response ($\boldsymbol{F}_{n+1}^p = \boldsymbol{F}_n^p$) without wrinkles or slacks ($a = 0, b = 0$).

4.2.1 Formation of slacks

Based on the elastic trial strains $[\boldsymbol{C}_r^e]^{\mathrm{tr}}$ the largest non-trivial eigenvalue of the tensor $[\boldsymbol{C}_r^e]^{\mathrm{tr}} - [\boldsymbol{C}_r^e]_{33}^{\mathrm{tr}} \, \boldsymbol{N}_3 \otimes \boldsymbol{N}_3$ is computed. Let this eigenvalue be denoted as λ_1. Then, the condition associated with the formation of slacks reads:

$$\text{if } \lambda_1 < 1, \text{ a slack forms and } \boldsymbol{C}_r^e = \boldsymbol{1}, \ \boldsymbol{S} = \boldsymbol{0}, \ \boldsymbol{F}_{n+1}^p = \boldsymbol{F}_n^p, \ \boldsymbol{\kappa}_{n+1} = \boldsymbol{\kappa}_n. \tag{54}$$

Since the arguments leading to Condition (54) are identical to those for hyperelastic solids, further details are omitted. They may be found in [15].

4.2.2 Standard elastic response without wrinkles or slacks

If Condition (54) is not fulfilled, the formation of wrinkles is checked subsequently. For that purpose, the standard solution (no additional plastic deformations and no

wrinkles or slacks) is required. It is computed from the local minimization problem

$$\lambda_3^C = \arg\inf_{\lambda_3^C} \Psi_{n+1}(\lambda_3^C) \tag{55}$$

with $a = 0$, $b = 0$ and $\boldsymbol{F}_{n+1}^{\mathrm{p}} = \boldsymbol{F}_n^{\mathrm{p}}$, $\boldsymbol{\kappa}_{n+1} = \boldsymbol{\kappa}_n$. Finally, the stresses follow from

$$\bar{\boldsymbol{S}} = 2\,\partial_{\boldsymbol{C}_{\mathrm{r}}^{\mathrm{e}}}\hat{\Psi}, \qquad \text{with } \hat{\Psi} = \inf_{\lambda_3^C} \Psi_{n+1}(\lambda_3^C). \tag{56}$$

As shown before, the resulting stress state is plane. In the following, the two non-trivial eigenvalues of $\bar{\boldsymbol{S}}$ are denoted as $\bar{S}_1$ and $\bar{S}_2$ with $\bar{S}_1 > \bar{S}_2$.

4.2.3 Wrinkling without additional plastic deformation

It is important to note that due to the interplay between plastic effects and the formation of wrinkles one cannot estimate if wrinkling occurs by using only the standard solution according to Subsection 4.2.2. Consequently, a second predictor-corrector step is applied. More precisely, it is assumed that the considered loading step is purely elastic ($\boldsymbol{F}_{n+1}^{\mathrm{p}} = \boldsymbol{F}_n^{\mathrm{p}}$, $\boldsymbol{\kappa}_{n+1} = \boldsymbol{\kappa}_n$). In this case, the wrinkling condition simplifies to

$$\text{if } \bar{S}_2 < 0, \text{ wrinkling occurs} \tag{57}$$

cf. [15]. If Condition (57) is fulfilled, the solution associated with the corrector step is obtained from

$$(a, \alpha, \lambda_3^C) = \arg\inf_{a,\alpha,\lambda_3^C} \Psi_{n+1}(a, \alpha, \lambda_3^C) \tag{58}$$

and the stresses are again given by Eq. (56) where $\hat{\Psi}$ is the reduced minimization problem resulting from Eq. (58).

4.2.4 Plastic deformations without wrinkles or slacks

Based on the predictor steps according to Subsections 4.2.2 or 4.2.3 the discrete loading condition is checked, i.e,

$$\phi^{\mathrm{tr}} = \phi(\boldsymbol{\Sigma}_{n+1}, \boldsymbol{Q}(\boldsymbol{\kappa}_n)) > 0. \tag{59}$$

If this inequality is not fulfilled, the predictor already represents the physical solution. Otherwise a plastic corrector is required. In case of a predictor without wrinkles, the corrector is defined by the local optimization problem (26). Clearly, the

16

transversal strain component λ_3^C has to be included in the minimization problem to guarantee plane stress conditions. It is noteworthy that although the predictor step does not show wrinkles, the converged corrector may fulfill condition (57). In this case an additional corrector as described in the next subsection is necessary.

4.2.5 Plastic deformations combined with wrinkling

If the plastic corrector as presented in Subsection 4.2.4 corresponds to wrinkling (Ineq. (57)), or if the wrinkled state according to Subsection 4.2.3 is associated with plastic loading (Ineq. (59)), the fully coupled minimization problem (50) has to be solved numerically (with $b = 0$).

4.2.6 Resulting algorithm

The resulting algorithm is summarized in Fig. 1 As mentioned before, due to the
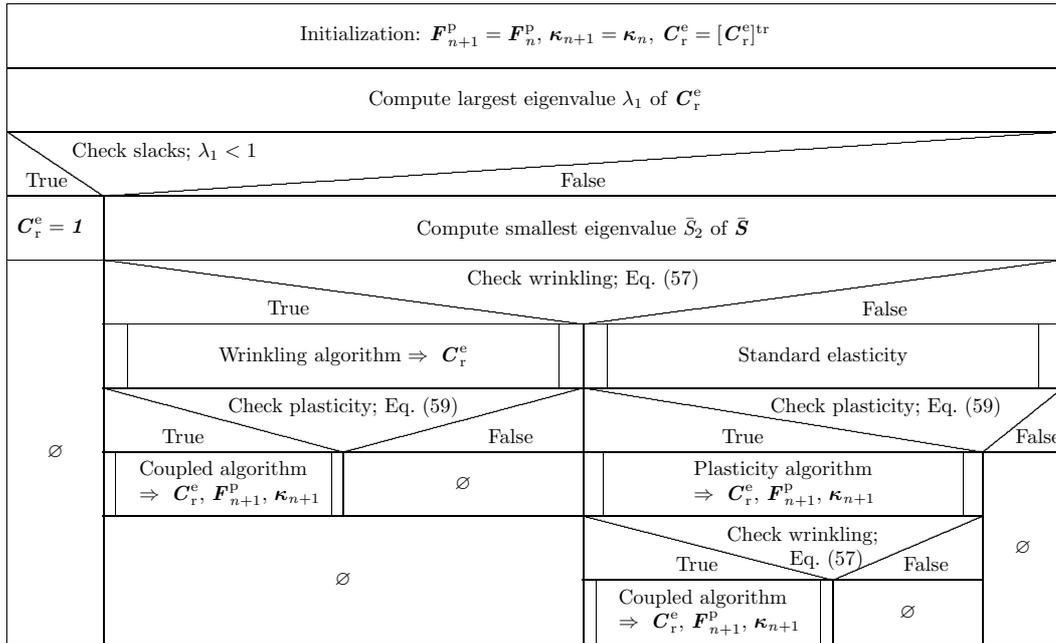

Fig. 1. Flow chart of the variationally consistent algorithm for wrinkling in inelastic membranes

interplay between wrinkling and plastic deformation, the predictor (53) is not sufficient to estimate whether the resulting state is characterized by plasticity, wrinkling or by both phenomena. Therefore, one additional wrinkling check is required.

17

4.3 Numerical implementation for fully isotropic models

If Ψ^{e} as well as ϕ are isotropic tensor functions, the numerical implementation can be significantly simplified. Clearly, the solution associated with the standard case (no plasticity and no wrinkles or slacks) or that corresponding to the formation of slacks can be obtained straightforward. On the other hand, if only wrinkling occurs (no additional plastic deformation), the wrinkling direction is known in advance, cf. Remarks 1. More precisely, only a scalar-valued minimization depending on the parameter a has to be solved. In case of plasticity, coaxiality between the predictor step and the converged solution can be used, cf. Remark 2, i.e., a return-mapping in principal axes, refer to [29]. As a consequence, the only remaining case is the fully coupled one (wrinkling combined with plastic effects).

However, it can be shown in a relatively straightforward manner that even in the coupled case, the relaxed elastic right Cauchy-Green tensor $\boldsymbol{C}_{\mathrm{r}}^{\mathrm{e}}$ is coaxial to its trial counterpart. More precisely, with the spectral decomposition of the elastic trial strains

$$[\boldsymbol{C}_{\mathrm{r}}^{\mathrm{e}}]^{\mathrm{tr}} = \sum_{i=1}^{3} \left(\lambda_i^{\boldsymbol{C}_{\mathrm{r}}^{\mathrm{etr}}} \right)^2 \, \boldsymbol{N}_i \otimes \boldsymbol{N}_i \tag{60}$$

and enforcing $\lambda_1^{\boldsymbol{C}_{\mathrm{r}}^{\mathrm{e}}} > \lambda_2^{\boldsymbol{C}_{\mathrm{r}}^{\mathrm{e}}} = \lambda_3^{\boldsymbol{C}_{\mathrm{r}}^{\mathrm{e}}}$ which follows from isotropy of Ψ^{e} together with the uniaxial stress state characterizing wrinkling, the wrinkling related tensor $\boldsymbol{C}_{\mathrm{w}}$ shows the form

$$\boldsymbol{C}_{\mathrm{w}} = a^2 \, \boldsymbol{N}_2 \otimes \boldsymbol{N}_2. \tag{61}$$

Here, $\boldsymbol{N}_2$ represents the wrinkling direction and $\boldsymbol{N}_3$ denotes the normal of the membrane. As a result, the spectral decomposition of $\boldsymbol{C}_{\mathrm{r}}^{\mathrm{e}}$ can be written as

$$\begin{aligned}[\boldsymbol{C}_{\mathrm{r}}^{\mathrm{e}}]_{n+1} := \quad & \left(\lambda_1^{\boldsymbol{C}_{\mathrm{r}}^{\mathrm{etr}}} \right)^2 \exp[-2 \, \Delta\lambda_1^{\mathrm{p}}] \, \boldsymbol{N}_1 \otimes \boldsymbol{N}_1 \\ & + \left[\left(\lambda_2^{\boldsymbol{C}_{\mathrm{r}}^{\mathrm{etr}}} \right)^2 \exp[-2 \, \Delta\lambda_2^{\mathrm{p}}] + a^2 \right] \, [\boldsymbol{1} - \boldsymbol{N}_1 \otimes \boldsymbol{N}_1]. \end{aligned} \tag{62}$$

Again, $\Delta\lambda_i^{\mathrm{p}}$ are the eigenvalues of $\Delta\lambda \, \boldsymbol{K}$, i.e.,

$$\Delta\lambda \, \boldsymbol{K} = \sum_{i=1}^{3} \Delta\lambda_i^{\mathrm{p}} \, \boldsymbol{N}_i \otimes \boldsymbol{N}_i \tag{63}$$

cf. Remark. 2. As a result, the minimization problem (50) with $b = 0$ reduces to

$$(\Delta\lambda_1^{\mathrm{p}}, \Delta\lambda_2^{\mathrm{p}}, a) = \arg \inf_{\Delta\lambda_1^{\mathrm{p}}, \Delta\lambda_2^{\mathrm{p}}, a} \left\{ \Psi_{n+1}(\Delta\lambda_1^{\mathrm{p}}, \Delta\lambda_2^{\mathrm{p}}, a) - \Psi_n + \sigma_0 \, \Delta\lambda(\Delta\lambda_1^{\mathrm{p}}, \Delta\lambda_2^{\mathrm{p}}) \right\}. \tag{64}$$

Here, isotropic hardening of the type $\kappa_{n+1} = \kappa_n + f(\Delta\lambda_1^{\mathrm{p}}, \Delta\lambda_2^{\mathrm{p}})$ has been assumed.

Clearly, different solution schemes can be used to solve the minimization problem (64). In the present paper, a limited memory BFGS method [32] is applied. It requires the gradient of the function

$$\tilde{\Psi}(\Delta\lambda_1^{\mathrm{p}}, \Delta\lambda_2^{\mathrm{p}}, a) := \{\Psi_{n+1}(\Delta\lambda_1^{\mathrm{p}}, \Delta\lambda_2^{\mathrm{p}}, a) - \Psi_n + \sigma_0\,\Delta\lambda(\Delta\lambda_1^{\mathrm{p}}, \Delta\lambda_2^{\mathrm{p}})\} \quad (65)$$

to be minimized. After a straightforward calculation it results in

$$\frac{\partial\tilde{\Psi}}{\partial a} = a\,[\bar{S}_2 + \bar{S}_3] \tag{66}$$

$$\frac{\partial\tilde{\Psi}}{\partial\Delta\lambda_1^{\mathrm{p}}} = -\left(\lambda_1^{\boldsymbol{C}_{\mathrm{r}}^{\mathrm{etr}}}\right)^2\,\exp[-2\,\Delta\lambda_1^{\mathrm{p}}]\,\bar{S}_1 + \frac{\partial\Psi^{\mathrm{p}}}{\partial\kappa}\,\frac{\partial\kappa}{\partial\Delta\lambda_1^{\mathrm{p}}} \tag{67}$$

$$\frac{\partial\tilde{\Psi}}{\partial\Delta\lambda_1^{\mathrm{p}}} = -\left(\lambda_2^{\boldsymbol{C}_{\mathrm{r}}^{\mathrm{etr}}}\right)^2\,\exp[-2\,\Delta\lambda_2^{\mathrm{p}}]\,[\bar{S}_2 + \bar{S}_3] + \frac{\partial\Psi^{\mathrm{p}}}{\partial\kappa}\,\frac{\partial\kappa}{\partial\Delta\lambda_2^{\mathrm{p}}}. \tag{68}$$

Again, $\bar{S}_i = \bar{\boldsymbol{S}} : (\boldsymbol{N}_i \otimes \boldsymbol{N}_i)$ are the eigenvalues of the second Piola-Kirchhoff-type tensor $\bar{\boldsymbol{S}} = 2\,\partial_{\boldsymbol{C}_{\mathrm{r}}^{\mathrm{e}}}\Psi^{\mathrm{e}}$. If Newton's method is to be applied, the second derivatives are necessary, too. They can be simply obtained by using

$$\frac{\partial\bar{S}_i}{\partial a} = a\,(\boldsymbol{N}_i \otimes \boldsymbol{N}_i) : \mathbb{C} : (\boldsymbol{1} - \boldsymbol{N}_1 \otimes \boldsymbol{N}_1)\,, \qquad \mathbb{C} = 4\,\partial_{\boldsymbol{C}_{\mathrm{r}}^{\mathrm{e}}\boldsymbol{C}_{\mathrm{r}}^{\mathrm{e}}}\Psi^{\mathrm{e}} \tag{69}$$

$$\frac{\partial\bar{S}_i}{\partial\Delta\lambda_1^{\mathrm{p}}} = -\left(\lambda_1^{\boldsymbol{C}_{\mathrm{r}}^{\mathrm{etr}}}\right)^2\,\exp[-2\,\Delta\lambda_1^{\mathrm{p}}]\,(\boldsymbol{N}_i \otimes \boldsymbol{N}_i) : \mathbb{C} : (\boldsymbol{N}_1 \otimes \boldsymbol{N}_1) \tag{70}$$

$$\frac{\partial\bar{S}_i}{\partial\Delta\lambda_2^{\mathrm{p}}} = -\left(\lambda_2^{\boldsymbol{C}_{\mathrm{r}}^{\mathrm{etr}}}\right)^2\,\exp[-2\,\Delta\lambda_1^{\mathrm{p}}]\,(\boldsymbol{N}_i \otimes \boldsymbol{N}_i) : \mathbb{C} : (\boldsymbol{1} - \boldsymbol{N}_1 \otimes \boldsymbol{N}_1). \tag{71}$$

Obviously, for a quadratic convergence at structural level, the linearization of $\tilde{\Psi}$ with respect to the total strains $\boldsymbol{F}$ is required. However, it can be derived in standard manner. Therefore, further details are omitted.

4.4 Illustrative examples

For the sake of comprehensibility, two prototype models are presented in this subsection. While single slip plasticity theory is briefly presented in Subsection 4.4.1, Subsection 4.4.2 is concerned with a von Mises type plasticity model.
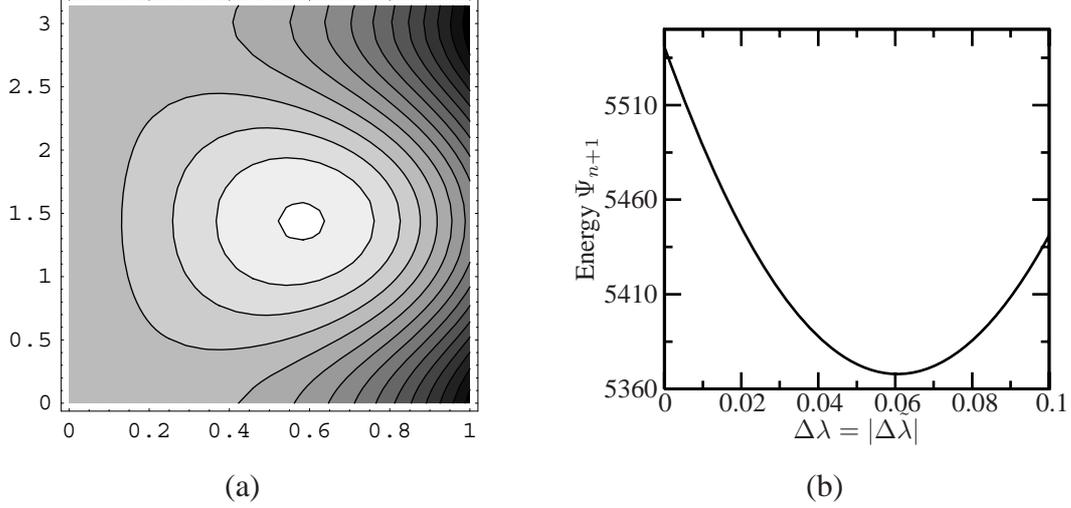
Fig. 2. Single slip plasticity; energy landscape of the incremental potential $\int_{t_n}^{t_{n+1}} \mathcal{E} \, dt$: (a) no plastic deformations; the potential depends only on the wrinkling parameters a (horizontal) and α (vertical), (b) no wrinkling

4.4.1 Example I: single slip system – Tresca's flow rule

If single slip plasticity theory is included in a membrane formulation, special attention is required to avoid inadmissible transverse shear strains. For that purpose, it is assumed that the slip system belongs to the tangent space of the membrane (with respect to the intermediate configuration). Hence, the out-of-plane response is purely elastic. On this account, it is convenient to enforce plane stress condition a priori. This can be archived by directly starting with a reduced elastic strain energy Ψ^e, cf. the Appendix in [15]. Consequently, Ψ^e used in the present Subsection 4.4.1 does not depend on λ_3^C anymore.

As mentioned before, in case of slacks, the local optimization problem (50) has a trivial solution, cf. Eq. (54). Thus, it is sufficient to consider the minimization problem

$$(\Delta\tilde{\lambda}, a, \alpha) = \arg \inf_{\Delta\tilde{\lambda}, a, \alpha} \left\{ \Psi_{n+1}(\Delta\tilde{\lambda}, a, \alpha) - \Psi_n + \sigma_0 \, |\Delta\tilde{\lambda}| \right\} \tag{72}$$

see Subsection 3.2. In a first step, the fully uncoupled cases are analyzed. While in Fig. 2(a) plastic effects are neglected, wrinkling is excluded in Fig. 2(b). Both figures are based on the same incremental potential. More precisely, a (two-dimensional) deformation gradient of the type

$$\boldsymbol{F} = \boldsymbol{1} + \frac{1}{2} \, \gamma \, (\tilde{\boldsymbol{n}} + \tilde{\boldsymbol{m}}) \otimes (\tilde{\boldsymbol{n}} - \tilde{\boldsymbol{m}}) + \varepsilon \, \boldsymbol{E}_1 \otimes \boldsymbol{E}_1 \tag{73}$$

with $\gamma = 0.5$ and $\varepsilon = -0.2$ is assumed. It correspond to a simple shear deformation superposed by a compression in $\boldsymbol{E}_1$ direction. For the elastic response, a
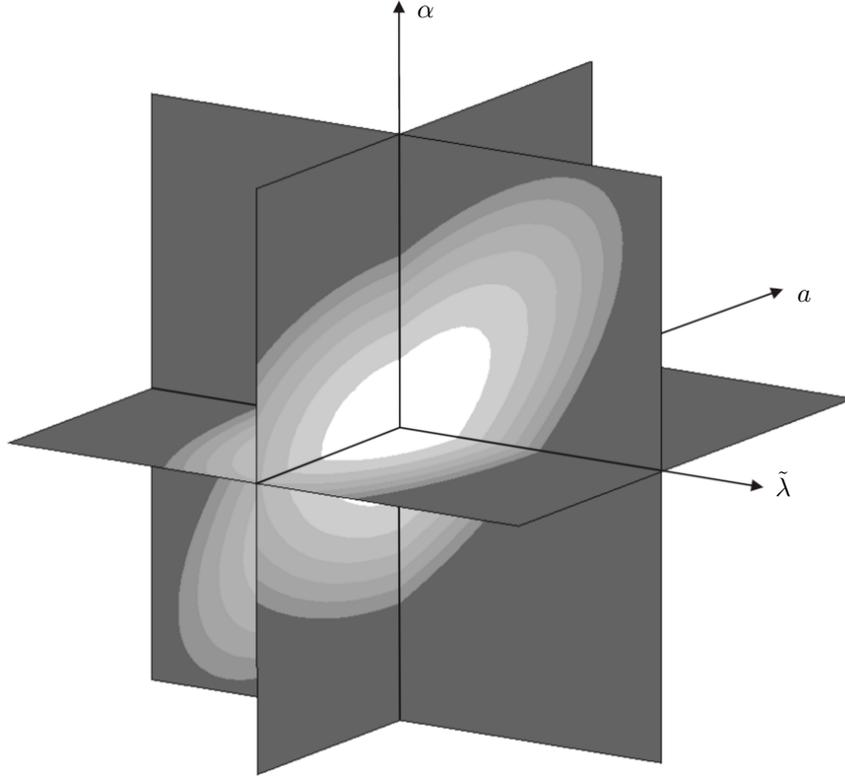
20

Fig. 3. Single slip plasticity; energy landscape of the incremental potential $\int_{t_n}^{t_{n+1}} \mathcal{E} \, \mathrm{d}t$ for the fully coupled case (wrinkling combined with plastic deformations)

two-dimensional neo-Hooke model is adopted, cf. the Appendix in [15]. Hardening effects are neglected, i.e., $\Psi^{\mathrm{p}} = 0$. According to Fig. 2, plasticity as well as wrinkling relax the physical problem, i.e., they result in an energy decrease. While wrinkling shows a significant impact on the energy (87% reduction in energy compared to the standard fully elastic case), plastic effects are comparably small (4% reduction in energy compared to the standard fully elastic case).

Next, the fully coupled problem is investigated. Clearly, the resulting energy has to be lower than (or equal to) that associated with uncoupled wrinkling. The computed energy landscape depending on the plastic slip $\Delta\tilde{\lambda}$ and the wrinkling parameters a and α is shown in Fig. 3. It bears emphasis that the yield function is not isotropic and hence, coaxiality between the elastic trial strains and the converged relaxed elastic strains is not fulfilled. As a result, the minimization problem (72) cannot be further simplified. Indeed, at the minimum as illustrated in Fig. 3 the wrinkling direction does not coincide with one of the eigenvectors of the elastic trial strains. The relaxed problem leads to a reduction in energy of about 88% compared to the standard, fully elastic solution. For the sake of comparison, the energies as predicted by the different schemes are summarized in Tab. 1.

21

Model	Energy [%]	Reduction in energy [%]
Standard	100	/
Plasticity	96	4
Wrinkling	13	87
Coupled	12	88

Table 1
Single slip plasticity; energies resulting from different models.

4.4.2 Example II: von Mises Plasticity

In contrast to single slip plasticity theory, the proposed von Mises type model is purely isotropic (Ψ^{e} as well as ϕ). Consequently, the algorithm as presented in Subsection 4.3 can be employed with the sole exception that the strain-like internal variable κ is replaced by the equivalent plastic strain ε^{p}. As a result, the function to be minimized reads

$$\tilde{\Psi}(\Delta\lambda_1^{p}, \Delta\lambda_2^{p}, a) = \{\Psi_{n+1}(\Delta\lambda_1^{p}, \Delta\lambda_2^{p}, a) - \Psi_n + \sigma_0\, \Delta\varepsilon^{p}(\Delta\lambda_1^{p}, \Delta\lambda_2^{p})\} \quad (74)$$

compare to Eq. (65). Here, the rate of the equivalent plastic strains depends on $\Delta\lambda_1^{p}$ and $\Delta\lambda_2^{p}$ according to Eq. (43). In line with the previous subsection, the elastic response is approximated by means of a hyperelastic neo-Hooke model. Isotropic hardening is accounted for by a linear function of the type $Q = Q(\varepsilon^{p})$ (hence, Ψ^{p} is quadratic). Since the model is fully isotropic, the eigenvectors of the elastic trial strains are irrelevant. Thus, $[C_r^{e}]^{tr}$ is defined by its eigenvalues $\lambda_1^{C_r^{etr}} = 2.0$ and $\lambda_2^{C_r^{etr}} = 0.2$.

Following the previous subsection, the uncoupled problems (plasticity or wrinkling) are analyzed first. It is noteworthy that in case of plastic deformations and vanishing wrinkles, the transversal strain λ_3^{C} has to be taken into account in the minimization problem. Again, the energy corresponding to the standard fully elastic problem without wrinkles can be significantly relaxed by plasticity or wrinkling. More precisely, wrinkling leads to a reduction in energy of about 70.5%, while plasticity results in a 99.3% reduction (compared to the standard elastic problem). If both relaxation phenomena are coupled, a further decrease in energy can be observed. The respective energy landscape is given in Fig. 4. Its minimum corresponds to to 99.7% reduction. For the sake of comparison, the energies as predicted by the different schemes are summarized in Tab. 2.
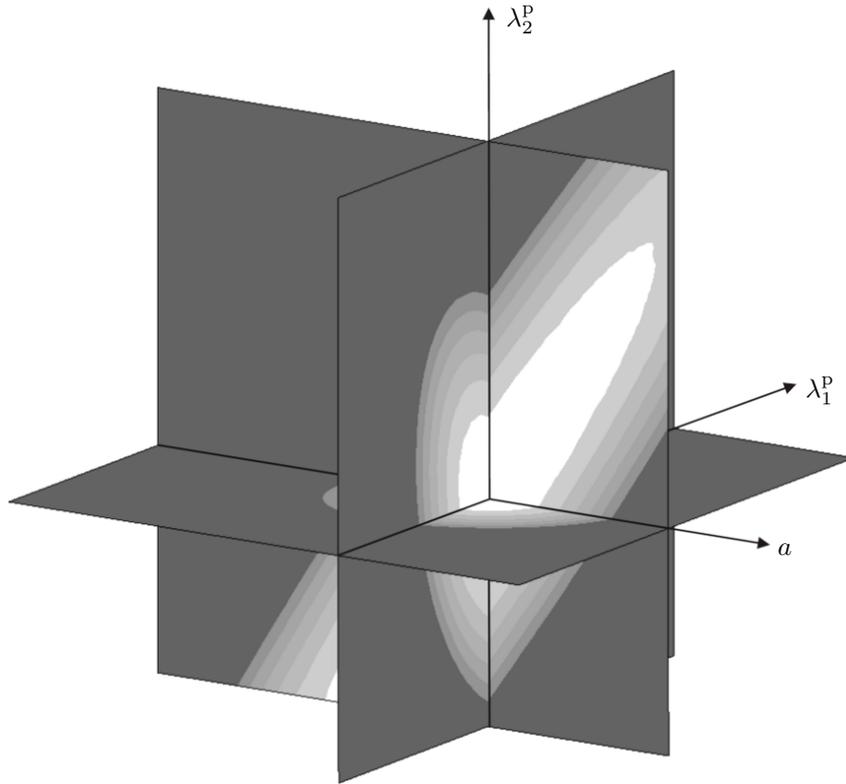
22

Fig. 4. Von Mises plasticity; energy landscape of the incremental potential $\tilde{\Psi}$ for the fully coupled case (wrinkling combined with plastic deformations)
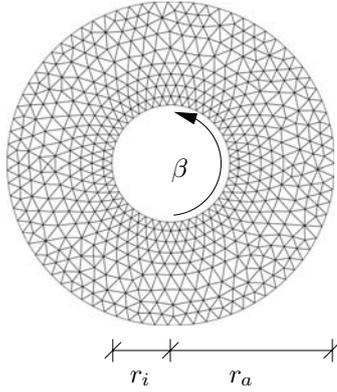
Model	Energy [%]	Reduction in energy [%]
Standard	100.0	/
Plasticity	0.7	99.3
Wrinkling	29.5	70.5
Coupled	0.3	99.7

Table 2
Von Mises plasticity model; energies resulting from different models.

5   Numerical example: Torsion of a circular membrane

In this section, the applicability as well as the performance of the advocated variational model for wrinkling in inelastic membranes is demonstrated by means of a selected numerical example. The considered example is concerned with a circular aluminum membrane subjected to torsion, Fig. 5. A similar problem has been investigated by several researchers, cf. e.g. [20,6,8]. Here, the geometry and the elastic material parameters are chosen according to [20]. The elastic free energy Ψ^e

Fig. 5. Torsion of an elastoplastic circular membrane: boundary conditions and material parameters. The membrane is clamped at both radii. The dimensions are $r_a = 125$ mm, $r_i = 45$ mm; the thickness is $t = 0.01$ mm.

Material parameters			
Elastic model; Eq. (75)		Plastic model; Subsection 3.3	
λ	40384.6 N/mm^2	σ_0	130.0 N/mm^2
μ	26923.1 N/mm^2	H	500.0 N/mm^2
		Ψ^{p}	$1/2 H \, (\varepsilon^{\mathrm{p}})^2$ (linear hardening)

is assumed to be of neo-Hooke type (see [33]), i.e.,

$$\Psi^{\mathrm{e}}(\boldsymbol{C}^{\mathrm{e}}) = \lambda \, \frac{(J^{\mathrm{e}})^2 - 1}{4} - \left(\frac{\lambda}{2} + \mu\right) \, \log J^{\mathrm{e}} + \frac{1}{2} \, \mu \, (\mathrm{tr}\boldsymbol{C}^{\mathrm{e}} - 3) \tag{75}$$

with

$$J^{\mathrm{e}} = \sqrt{\det \boldsymbol{C}^{\mathrm{e}}}, \qquad \mathrm{tr}\boldsymbol{C}^{\mathrm{e}} = \boldsymbol{C}^{\mathrm{e}} : \boldsymbol{1}. \tag{76}$$

The membrane having a thickness of $t = 0.01$mm is clamped at the outer as well as at the inner boundary and loading is applied by increasing the angle β at the inner boundary up to $\beta_{\max} = 1.8° = 0.03176$rad. Subsequently, the angle β is decreased up to $\beta = 0$rad. In contrast to introduced illustrative examples, the problem has been experimentally analyzed as well, cf. [20]. Due to the relatively large strains, plastic effects can be observed in the experiment. Hence, a plasticity model is needed to guarantee a realistic finite element approximation. Here, the von Mises model as summarized in Subsection 3.3 is adopted. Isotropic hardening is taken into account by a potential of the type, $\Psi(\varepsilon^{\mathrm{p}}) = 1/2 \, H(\varepsilon^{\mathrm{p}})^2$, with H being the (constant) hardening modulus. The material parameters characterizing an aluminum membrane are given in Fig. 5.

Based on the introduced, fully variational algorithmic formulation for inelastic membranes a finite element analysis of the circular membrane has been performed. The underlying spatial discretization is depicted in Fig. 5. It contains 1072 bi-quadratic 6 node triangular elements. Both the local wrinkling-related minimization problems according to Subsection 4.2 or 4.3 as well as the resulting global optimization problem (15) are solved by using the limited memory BFGS method [32].

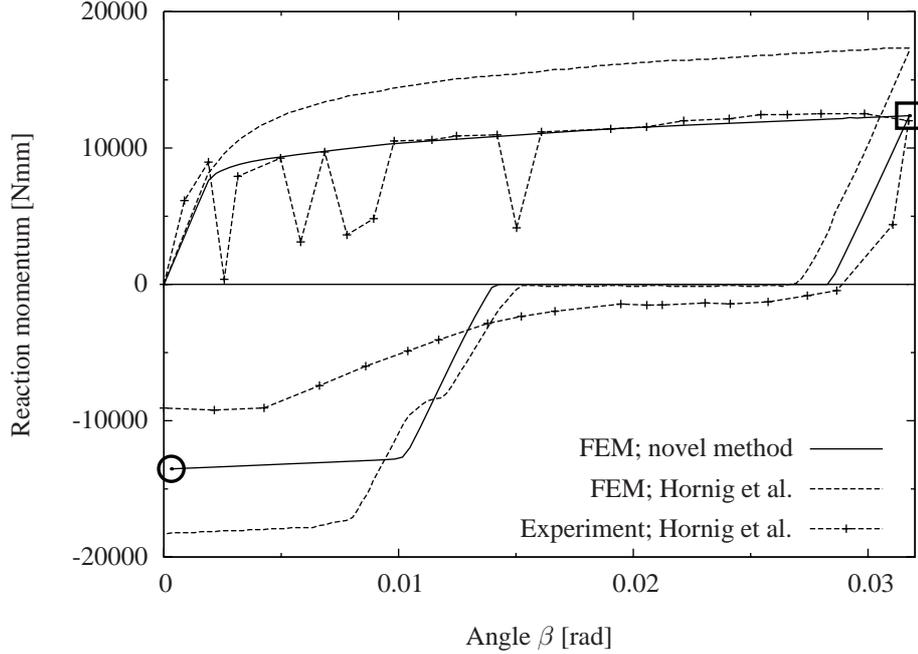The predicted reaction momentum vs. angle diagram is shown in Fig. 6. For the

Fig. 6. Torsion of an elastoplastic circular membrane: momentum vs. angle diagram

sake of comparison, the numerical results reported in [20], together with the experimentally observed structural behavior (cf. [20]), are also included. During the first loading stage (β is increased from 0 up to $\beta_{\max} = 1.8° = 0.03176$rad) the good agreement between the experiment and the novel algorithmic formulation is noteworthy. In contrast to the model by Hornig & Schoop the ultimate load (momentum) is not overestimated. However, although the novel results are significantly more realistic than those shown in [20] even during the second loading stage (β is decreased from $\beta_{\max} = 1.8° = 0.03176$rad up to 0), a slight difference compared to the experimentally determined curve is obvious. A careful analysis of the diagram reveals three possible explanations: (1) The experimental data seems to scatter; (2) The initially flat membrane is transformed into a corrugated plate during the loading stage which changes the structural stiffness of the membrane for the subsequent unloading and load reversal stage; (3) During unloading (β decreases and varies between 0.025rad and 0.015rad) the structure is not fully unloaded (non-vanishing momentum). Hence, kinematic hardening which is not included within the numerical model plays a non-negligible role. It bears emphasis that although only isotropic hardening is taken into account within the variational algorithm, the modifications necessary for the kinematic counterpart are straightforward, cf. [25–27].

The wrinkling directions and amplitudes, together with the plots of the equivalent plastic strain ε^{p} are summarized in Fig.7. The plots on the right hand side are associated with $\beta_{\max} = 0.03176$rad. It can be seen that, as expected, the wrinkles point into the loading direction. Furthermore, the inelastic strains are localized at the inner boundary. If the angle β is decreased, the amplitudes of the wrinkles also decrease first. However, at a certain stage and in contrast to the fully elastic problem,
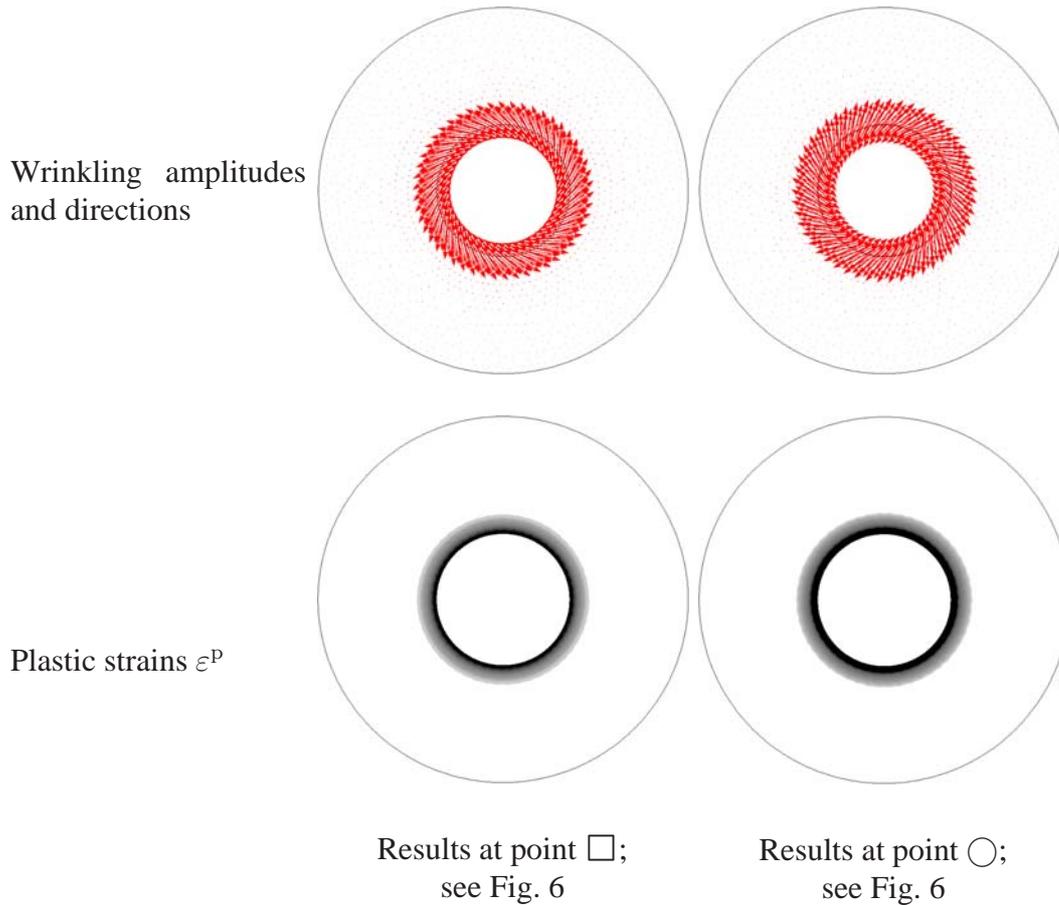
25

Wrinkling amplitudes and directions

Plastic strains ε^{p}

Results at point □;   Results at point ◯;
see Fig. 6   see Fig. 6

Fig. 7. Torsion of a circular membrane: distribution of the wrinkling strains and equivalent plastic strains ε^{p}. The plots on the left hand side are associated with $\beta_{\mathrm{max}} = 0.03176\mathrm{rad}$ (point □ in Fig. 6), while the plots on the right hand side correspond to the point ◯ in Fig. 6.

wrinkling in the current loading direction occurs. Furthermore, additional inelastic deformations can be observed. The wrinkling pattern is in good agreement with that reported in [20].

Interestingly, numerical problems have arisen in [20] during the computations. They have been reduced by deriving an initial guess for the employed Newton's scheme. It is noteworthy that such numerical problems have not been observed in the presented finite element formulation. Furthermore, even if numerical instabilities become dominant in the novel variational approach, a (standard) more sophisticated optimization method can be adopted without any additional effort, cf. [34].

6 Conclusion

In this paper, a novel, fully variational formulation suitable for wrinkling in inelastic membranes at finite strains was presented. The distinguishing character of

the new approach is that every aspect of the considered physical problem is driven by energy minimization. An introduction of ad-hoc loading conditions is not required, but they follow naturally from the mathematically and physically sound variational principle itself. Based on relaxing an incrementally defined energy functional, the plastic strains, the internal variables, together with the wrinkling patterns, are jointly computed. Furthermore, by doing so, a reduced functional depending only on the standard strains is derived which acts like a hyperelastic potential for the stresses. More precisely, the stresses result from differentiating this potential with respect to the strains. Consequently, the method is formally identical to standard hyperelasticity with the sole exception that the aforementioned potential is locally defined (in time).

In line with the theoretical part of the present paper, the proposed numerical implementation is based on the same variational structure, i.e., after applying a time discretization to the evolution equations, all unknown variables are computed by employing classical minimization algorithms. As a result, the numerical formulation is relatively straightforward and the resulting algorithm inherits the efficiency and robustness properties of the underlying optimization scheme. In particular for highly non-linear problems such as wrinkling in membranes this represents an important advantage of the advocated idea compared to previous approaches. It bears emphasis that the presented implementation does not rely on any symmetry assumptions concerning the elastic response or the yield function. For fully isotropic models, an adapted numerical implementation in principal stress space was derived.

In the present paper, only dissipative effects resulting from rate-independent plasticity have been considered. However, since many rate effects can also be described in a variationally consistent manner, cf. [25,35], their incorporation into the novel variational membrane model is relatively straightforward. The same holds true for the fully thermo-mechanically coupled problem, cf. [36].

References

[1] H. Wagner. Ebene Blechwandträger mit sehr dünnen Stegblechen. *Z. Flugtechnik u. Motorluftschiffahrt*, 20, 1929.

[2] E Reissner. On tension field theory. In *Fifth Int. Cong. on Appl. Mech.*, pages 88–92, 1938.

[3] D.G. Roddeman, J. Drukker, C.W.J. Oomens, and J.D. Janssen. The wrinkling of thin membranes: Part I – theory. *Journal of Applied Mechanics*, 54:884–887, 1987.

[4] D.G. Roddeman, J. Drukker, C.W.J. Oomens, and J.D. Janssen. The wrinkling of thin membranes: Part I – numerical analysis. *Journal of Applied Mechanics*, 54:888–892, 1987.

[5] H. Schoop, L. Taenzer, and J. Hornig. Wrinkling of nonlinear membranes. *Computational Mechanics*, 29:68–74, 2002.

[6] R. Rossi, M. Lazzari, R. Vitaliani, and E. Oñate. Simulation of light-weight membrane structures by wrinkling model. *International Journal for Numerical Methods in Engineering*, 62:2127–2153, 2005.

[7] T. Raible, K. Tegeler, S. Löhnert, and P. Wriggers. Development of a wrinkling algorithm for orthotropic membrane materials. *Computer Methods in Applied Mechanics and Engineering*, 194:2550–2568, 2005.

[8] M. Miyazaki. Wrinkle/slack model and finite element dynamics of membranes. *International Journal for Numerical Methods in Engineering*, 66:1179–1209, 2006.

[9] A. Jarasjarungkiat, R. Wuechner, and K.U. Bletzinger. A wrinkling model based on material modification for isotropic and orthotropic membranes. *Computer Methods in Applied Mechanics and Engineering*, 197:773–788, 2007.

[10] D.J. Steigmann. Tension-Field theory. *Proceedings of the Royal Society of London. Series A, Mathematical and Physical Science*, 429:141–173, 1990.

[11] A.C. Pipkin. The relaxed energy density for isotropic elastic membranes. *IMA Journal of Applied Mathematics*, 36:85–99, 1986.

[12] A.C. Pipkin. Convexity conditions for strain-dependent energy functions for membranes. *Arch. Rational Mech. Anal.*, 121:361–376, 1993.

[13] A.C. Pipkin. Relaxed energy densities for large deformations of membranes. *IMA Journal of Applied Mathematics*, 52:297–308, 1994.

[14] M. Epstein. On the wrinkling of anisotropic membranes. *Journal of Elasticity*, 55:99–109, 1999.

[15] J. Mosler. A novel variational algorithmic formulation for wrinkling at finite strains based on energy minimization: application to mesh adaption. *Computer Methods in Applied Mechanics and Engineering*, 2007. in press.

[16] Arthur Lyons. *Materials for Architects & Builders*. Butterworth-Heinemann, 3rd edition, 2006.

[17] Xi Wang and Jian Cao. On the prediction of side-wall wrinkling in sheet metal forming processes. *International Journal of Mechanical Sciences*, 42:2369–2394, 2000.

[18] Eran Sharon, Benoit Roman, and Harry L. Swinney. Geometrically driven wrinkling observed in free plastic sheets and leaves. *Physical Review E*, 75(4), 2007.

[19] J. Hornig. *Analyse der Faltenbildung in Membranen aus unterschiedlichen Materialien*. PhD thesis, Technische Universität Berlin, 2004.

[20] J. Hornig and H. Schoop. Wrinkling analysis of membranes with elastic-plastic material behavior. *Computational Mechanics*, 35:153–160, 2005.

[21] J. Mosler and M. Ortiz. On the numerical implementation of variational arbitrary Lagrangian-Eulerian (VALE) formulations. *International Journal for Numerical Methods in Engineering*, 67:1272–1289, 2006.

[22] J. Mosler and M. Ortiz. h-adaption in finite deformation elasticity and plasticity. *International Journal for Numerical Methods in Engineering*, 2006. in press.

[23] J. Mosler. *On the numerical modeling of localized material failure at finite strains by means of variational mesh adaption and cohesive elements*. Habilitation, Ruhr University Bochum, Germany, 2007.

[24] F. Cirak and M. Ortiz. Fully c_1-conforming subdivision elements for finite deformation thin-shell analysis. *International Journal for Numerical Methods in Engineering*, 51:813–833, 2001.

[25] M. Ortiz and L. Stainier. The variational formulation of viscoplastic constitutive updates. *Computer Methods in Applied Mechanics and Engineering*, 171:419–444, 1999.

[26] M. Ortiz. Computational Solid Mechanics – Lecture Notes. *California Institute of Technology*, 2002.

[27] C. Carstensen, K. Hackl, and A. Mielke. Non-convex potentials and microstructures in finite-strain plasticity. *Proc. R. Soc. Lond. A*, 458:299–317, 2002.

[28] B. Halphen and Q.S. Nguyen. Sur les matériaux standards généralisés. *J. Méchanique*, 14:39–63, 1975.

[29] J.C. Simo. Numerical analysis of classical plasticity. In P.G. Ciarlet and J.J. Lions, editors, *Handbook for numerical analysis*, volume IV. Elsevier, Amsterdam, 1998.

[30] J. Alberty, C. Carstensen, and D. Zarrabi. Adaptive numerical analysis in primal elastoplasticity with hardening. *Computer Methods in Applied Mechanics and Engineering*, 171:175–204, 1999.

[31] J.C. Simo and T.J.R. Hughes. *Computational inelasticity*. Springer, New York, 1998.

[32] D.C. Liu and J. Nocedal. On the limited memory method for large scale optimization. *Mathematical Programming B*, 45(3):503–528, 1989.

[33] P. Ciarlet. *Mathematical elasticity. Volume I: Three-dimensional elasticity*. North-Holland Publishing Company, Amsterdam, 1988.

[34] C. Geiger and C. Kanzow. *Numerische Verfahren zur Lösung unrestringierter Optimierungsaufgaben*. Springer, 1999.

[35] E. Fancello, J.-P. Ponthot, and L. Stainier. A variational formulation of constitutive models and updates in non-linear finite viscoelasticity. *International Journal for Numerical Methods in Engineering*, 2005. in press.

[36] Q. Yang, L. Stainier, and M. Ortiz. A variational formulation of the coupled thermo-mechanical boundary-value problem for general dissipative solids. *Journal of the Mechanics and Physics of Solids*, 33:2863–2885, 2005.

29